Circumferential Tube Skin Temperature Profiles in Thermal Cracking Coils

G. J. Heynderickx, G. G. Cornelis, and G. F. Froment
Laboratorium voor Petrochemische Techniek, Rijksuniversiteit Gent, B9000 Gent, Belgium

Uniform temperature distributions in cracking furnaces favor the run length of the production cycle of the furnace and the tube metal life. The coupled simulation of the furnace and the reactor tubes by means of the zone method is extended to permit the calculation of circumferential nonuniformities under reaction conditions. Circumferential tube skin temperatures were found to vary over 50°C and more, due to "shadow effects." As a result, nonuniform coking rates and coke layers are obtained. The model and computational scheme presented here can be used as a guide for plant operators and as a tool for designing.

Introduction

Olefins, which are major building blocks of the petrochemical industry, are produced by thermal cracking in long tubular reactors, suspended in large, gas fired furnaces.

The configuration of the reactor coil, consisting of a number of straight vertical tubes called passes connected by bends, and the positioning and type of the burners require special attention. Hot spots can damage the tube material and lead to local excessive coke formation, thus reducing the normal run length of the production cycle. Uniform temperatures are recommended, not only in the axial direction of the tubes, but also along the tube perimeter. Since heat is mainly transmitted by radiation at the high temperatures required by the operation, special care has to be taken to maximize the incidence of direct radiation from the flames on the coils and to minimize the shadow effects.

Until now the evaluation of the importance of circumferential nonuniformities on the tube skin has not been solved in a satisfactory manner.

The Crossed-String method (Hottel, 1931) leads to approximate results only, because of the simplifications introduced in the modeling of heat transfer by radiation: absorption and (re-) emission of radiation by the flue gas, reflection of radiation by the tube skin and furnace walls, and conduction along the tube perimeter are not accounted for.

More recently, the coupled simulation of the firebox and reactor by means of the zone method, introduced by Hottel and Sarofim (1967) was further developed by Vercammen and Froment (1978, 1980); Rao et al. (1988) and Plehiers and Froment (1989) into a flexible package of simulation programs describing radiative and convective heat-transfer mechanisms in the furnace. In this approach the furnace and the reactor coils are discretized into a number of zones by means of planes parallel to the furnace walls. Energy balances permit the calculation of the temperature of each volume and surface zone and the heat fluxes between these zones.

In this article the simulation model is further extended to permit a rigorous calculation of the circumferential nonuniformities under reaction conditions. This required further discretization, now along the tube perimeter. Simulation results are given for an ethane cracking furnace with a single row of vertical tubes and for a naphtha cracking furnace with staggered rows of tubes.

Model Equations and Simulation Procedure

Reactor model

A one-dimensional plug flow model is used to simulate the thermal cracking reactor. Reynolds numbers of the order of 250,000 are calculated. The turbulence wipes out any process gas temperature profile over a cross-section of the reactor tubes.

The set of continuity equations for the process gas species is solved simultaneously with the energy equation and the pressure drop equation (Froment and Bischoff, 1990):

$$\frac{dF_j}{dz} = \left(\sum_i n_{ij} r_{ri}\right) \frac{\pi d_t^2}{4} \tag{1}$$

$$\sum_j F_j c_{pj} \frac{dT}{dz} = Q(z) \pi d_t + \frac{\pi d_t^2}{4} \sum_i r_{ri} (-\Delta H)_i \tag{2}$$

$$\left[\frac{1}{M_m p_t}-\frac{p_t}{\alpha G^2 RT}\right]\frac{dp_t}{dz}=\frac{d}{dz}\left(\frac{1}{M_m}\right)+\frac{1}{M_m}\left(\frac{1}{T}\frac{dT}{dz}+Fr\right) \quad (3)$$

with:

$$Fr=0.092\frac{Re^{-0.2}}{d_t} \quad (4)$$

for the straight parts of the reactor tubes, and:

$$Fr=0.092\frac{Re^{-0.2}}{d_t}+\frac{\xi}{\pi R_b} \quad (5)$$

for the tube bends, where:

$$\xi=\left(0.7+0.35\frac{\Lambda}{90°}\right)\left(0.051+0.19\frac{d_t}{R_b}\right) \quad (6)$$

The kinetics are based on a detailed radical reaction scheme (Froment, 1981 and Willems and Froment, 1988).

The scheme contains the complete reaction networks for the decomposition of the feed components (paraffins, naphtenics and aromatics) through initiation and hydrogen abstraction. The produced radicals isomerize and decompose. The disappearance of intermediates like large olefins and diolefins through initiation, H° and CH_3° radical addition and hydrogen abstraction is also accounted for in the networks. The latter have been generated by computer and contain over 10,000 radical reactions (Clymans and Froment, 1984; Hillewaert et al., 1988).

Furnace model

The furnace walls, the tube skins and the flue gas volume are divided into a number of isothermal surface and volume elements with uniform properties. The energy balance, containing contributions of radiative, convective and/or conductive heat exchange, is constructed for each of these elements, resulting in a set of nonlinear algebraic equations:

$$\begin{bmatrix} Z_1Z_1-\sum Z_1Z_j & Z_2Z_1 & \cdots & Z_nZ_1 \\ Z_1Z_2 & Z_2Z_2-\sum Z_2Z_j & \cdots & Z_nZ_2 \\ \vdots & \vdots & \vdots & \vdots \\ Z_1Z_n & Z_2Z_n & \cdots & Z_nZ_n-\sum Z_nZ_j \end{bmatrix}\begin{bmatrix} E_1 \\ E_2 \\ \vdots \\ E_n \end{bmatrix}=\begin{bmatrix} Q_1A_1 \\ Q_2A_2 \\ \vdots \\ Q_nA_n \end{bmatrix} \quad (7)$$

The matrix element Z_iZ_j represents the total exchange area between the zones Z_i and Z_j. This is the amount of radiative energy emitted by the zone Z_i and absorbed, both directly and after reflection on other zones, by the zone Z_j, divided by the black body emissive power E_i. The emissive power of a black body with temperature T_i is given by the Stefan-Boltzmann law $E_i=\sigma T_i^4$. The calculation of the total exchange areas for the flue gas volumes, the furnace wall zones, the tube skin zones and burners was discussed in detail by Rao et al. (1988) and by Plehiers and Froment (1989). The nonradiative heat flux emitted by the zone Z_i is represented by Q_i.

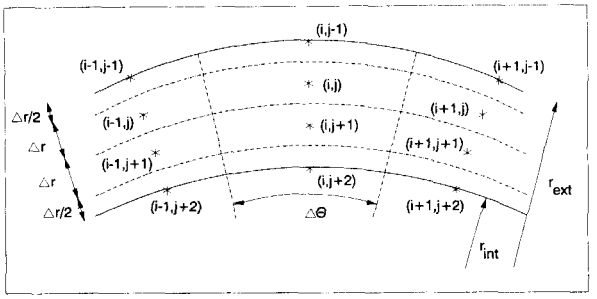

Figure 1. Tube wall grid.

Solving this set of energy balances yields the heat flux and the temperature distribution in the furnace. When the reactor tubes are discretized in axial direction only, heat flux profiles $q(z)$ and external tube skin temperature profiles $T_{ext}(z)$ are obtained. When the tubes are also discretized along the perimeter, heat flux profiles $q(\theta_j, z_i)$ and the corresponding tube skin temperature profiles $T_{ext}(\theta_j, z_i)$ are obtained.

As a result of the circumferential discretization of the tubes the heat transfer through the tube wall is no longer a one-dimensional problem. Next to the radial conduction of heat through the tube wall, circumferential heat conduction has to be considered as well.

The temperature in the tube wall and on its external and internal surface is calculated by dividing the tube wall into a grid of finite elements (Figure 1) and by setting up the energy equation for each of these elements.

The energy equation for the element $(i, j-1)$ on the external tube skin contains two contributions of circumferential conductive heat exchange with the elements $(i-1, j-1)$ and $(i+1, j-1)$, one contribution of radial conductive heat exchange with the element (i, j) and a contribution of heat received from the furnace:

$$\frac{\lambda}{r_{ext}\Delta\theta}\frac{\Delta r}{2}\Delta z(T_{i-1,j-1}+T_{i+1,j-1}-2T_{i,j-1})+\frac{\lambda}{\Delta r}\left(r_{ext}-\frac{\Delta r}{2}\right)\Delta\theta\,\Delta z(T_{i,j}-T_{i,j-1})+q(i)\,r_{ext}\Delta\theta\,\Delta z=0 \quad (8)$$

The energy equation for the element (i, j) in the tube wall contains two contributions of circumferential conductive heat

exchange with the elements $(i-1, j)$ and $(i+1, j)$ and two contributions of radial conductive heat exchange with the elements $(i, j-1)$ and $(i, j+1)$:

$$\frac{\lambda}{(r_{ext}-\Delta r)\Delta\theta}\Delta r\,\Delta z(T_{i-1,j}+T_{i+1,j}-2T_{i,j}) + \frac{\lambda}{\Delta r}\left(r_{ext}-\frac{\Delta r}{2}\right)\Delta\theta\,\Delta z(T_{i,j-1}-T_{i,j}) + \frac{\lambda}{\Delta r}\left(r_{ext}-\frac{3\Delta r}{2}\right)\Delta\theta\,\Delta z(T_{i,j+1}-T_{i,j})=0 \quad (9)$$

The energy equation for the element $(i, j+1)$ is completely analogous to that of the element (i, j).

The energy equation for the element $(i, j+2)$ on the internal tube skin contains two contributions of circumferential conductive heat exchange with the elements $(i-1, j+2)$ and $(i+1, j+2)$, one contribution of radial conductive heat exchange with the element $(i, j+1)$ and the contribution of convective heat exchange with the process gas at temperature T_p:

$$\frac{\lambda}{r_{int}\Delta\theta}\frac{\Delta r}{2}\Delta z(T_{i-1,j+2}+T_{i+1,j+2}-2T_{i,j+2}) + \frac{\lambda}{\Delta r}\left(r_{int}+\frac{\Delta r}{2}\right)\Delta\theta\,\Delta z(T_{i,j+1}-T_{i,j+2}) + h_p r_{int}\Delta\theta\,\Delta z(T_p-T_{i,j+2})=0 \quad (10)$$

The conductivity λ of the tube wall material is a temperature dependent value. In order to obtain a set of equations which are linear in the temperatures $T_{i,j}$, a conductivity value based on the average tube wall temperature is used.

The Eqs. 8, 9 and 10 are obtained by discretizing the conduction equation for each axial tube zone with the appropriate boundary conditions:

$$\nabla^2 T=\frac{d^2T}{dr^2}+\frac{1}{r}\frac{dT}{dr}+\frac{1}{r^2}\frac{d^2T}{d\theta^2}=0 \quad (11)$$

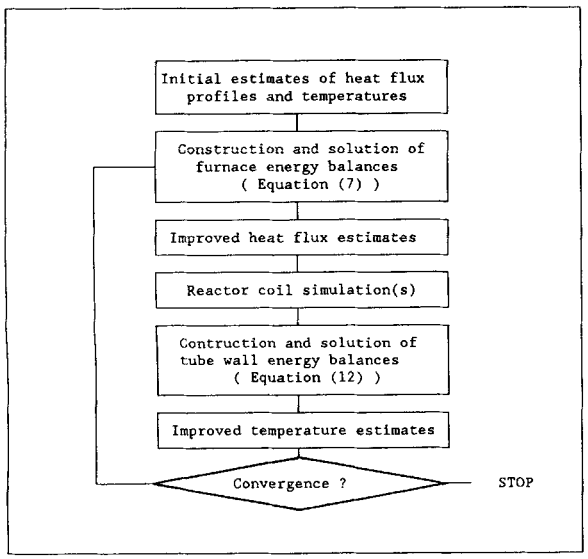

Figure 2. Flow chart of the calculations.

$$\lambda\nabla T(\theta, r)=q(\theta, r) \qquad r=r_{ext};\ V\theta$$

$$\lambda\nabla T(\theta, r)=h_p[T(\theta, r)-T_p] \qquad r=r_{int};\ V\theta$$

The set of Eqs. 8, 9 and 10 can be written as:

$$\underline{A}\,\underline{T}=\underline{B} \quad \text{from which:} \quad \underline{T}=\underline{A}^{-1}\underline{B} \quad (12)$$

The calculation module for the circumferential temperature profiles is coupled to the furnace simulation model FURNACE (Plehiers and Froment, 1989) and the reactor simulation model CRACKSIM (Willems and Froment, 1988). A simplified flow chart of the iterative calculation procedure is given in Figure 2.

Simulation of an Ethane Furnace with a Single Row of Coils

Furnace description

Ethane crackers frequently contain 4 parallel coils on a single row. Because of the symmetry and to save computer time only half a furnace was considered.

The main dimensions and operating conditions of the ethane cracker with a single row configuration are given in Table 1. Figures 3 and 4 present a top and a front view of the furnace. Each coil makes eight passes through the furnace. The furnace is heated by 64 burners positioned in eight rows of four burners in the front (A) and the rear (C) wall of the furnace.

The furnace was divided into zones by means of four equidistant horizontal planes. The five axial zones on each pass of

Table 1. Characteristics of the Ethane Cracking Furnace

Furnace	
Length	4,652 mm
Height	13,450 mm
Width	2,100 mm
Refractory thickness	230 mm
Insulation thickness	50 mm
Number of side wall burners	64
Firing Conditions	
Total heat input	16.53 MW
Reactor	
2 coils on a single row	
Total coil length	102,336 mm
Number of passes	8
Internal diameter of passes 1-6	124 mm
Internal diameter of passes 7-8	136 mm
Wall thickness	8 mm
Operating Conditions	
Feedstock	100% ethane
Hydrocarbon feed rate per coil	3,657 kg/h
Steam dilution	0.332
Coil inlet temperature	660°C
Coil outlet pressure	1.2 atm
Material Properties	
Emissivity of furnace wall	0.60
Emissivity of the tubes	0.95
Thermal conductivity of the	
refractory (W/m·K)	$0.0193+118.0\times10^{-6}\,T$(K)
insulation (W/m·K)	$0.0452+111.1\times10^{-6}\,T$(K)
tubes (W/m·K)	$-8.432+3.040\times10^{-2}\,T$(K)

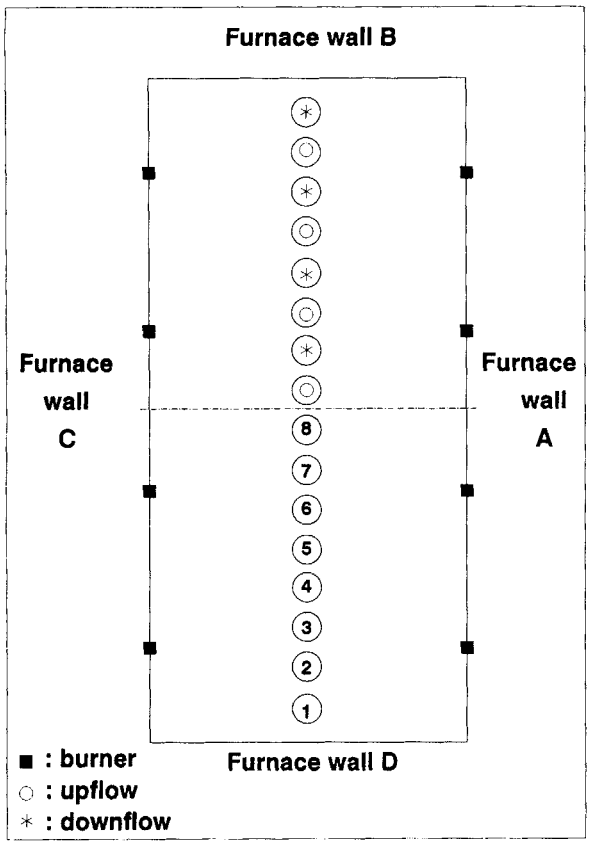

Figure 3. Top view of the ethane furnace.

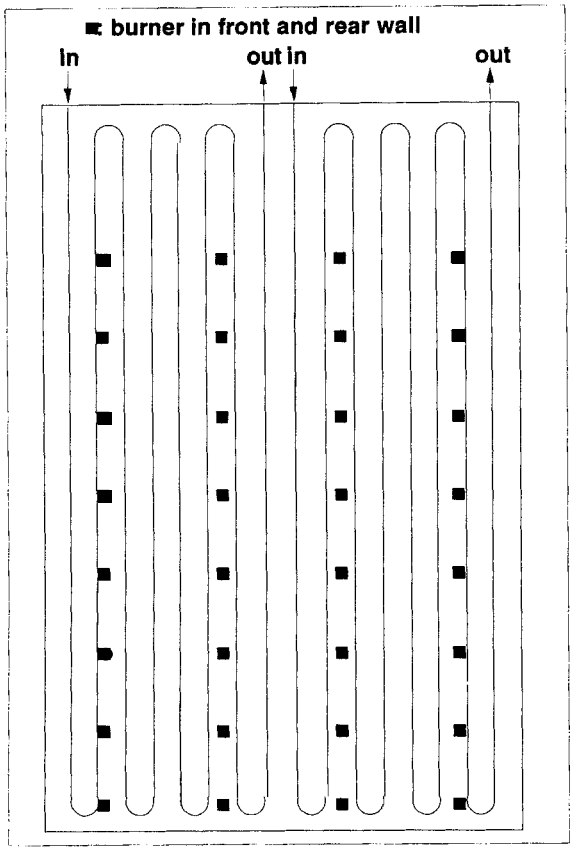

Figure 4. Front view of the ethane furnace.

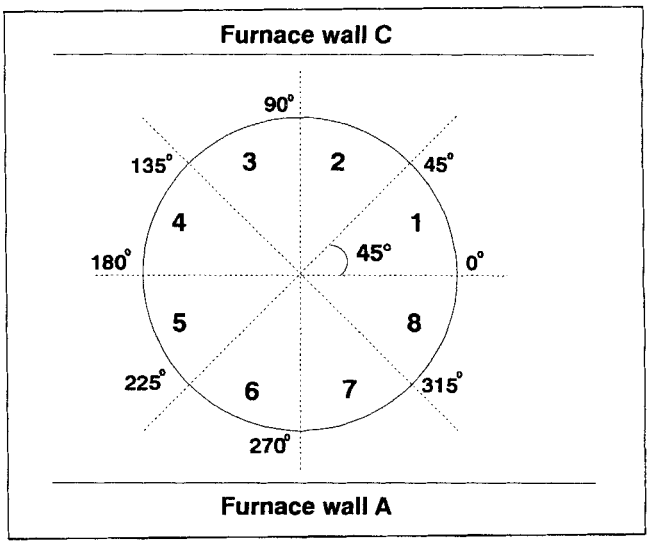

Figure 5. Circumferential discretization of tube.

the reactor coil, resulting from this discretization, were circumferentially divided into eight equal zones, as shown in Figure 5. For reasons of symmetry, only four of these circumferential zones had to be considered for each axial zone, leading to a total of 160 external tube skin zones, 12 furnace wall zones and 5 gas volume zones. The calculations were performed on the Data General AViiON 4120 (34 Mips).

Results and Discussion

Cracking furnaces are controlled on the basis of the process gas exit temperature and/or composition. Thermocouples inserted in intermediate locations of the coil do not last very long because of the severe operating conditions. This is why the external tube skin temperature is measured periodically by radiation pyrometers, through peepholes in the furnace walls. The simulation results presented here provide evidence that the observed temperature depends upon the location of the peephole with respect to the tube.

Circumferential nonuniformities are of particular importance for severe operating conditions, whereby the tube skin temperature is high and close to the limits imposed by the tube material properties. Therefore, a representative tube skin temperature is a necessity and the measurements should be correctly interpreted.

Figures 6 and 7 present the internal and external circumferential tube skin temperature profiles at the height of 4 m from the furnace floor, for respectively the third and eighth pass of the reactor coil. The external tube skin temperature of the third tube varies over 43°C from 887°C and 930°C. The variation in internal tube skin temperature is less pronounced because of the circumferential conduction of heat through the tube wall, but it still amounts to 33°C. The temperature profiles have 2 maxima and 2 minima. The maximum temperatures are located on the circumferential zones 6 and 7 (Figure 5), directly facing the front wall A, and on the zones 2 and 3, directly facing the rear wall C of the furnace. These zones receive direct radiation from the furnace walls and the burners. The minimum temperatures occur in the plane of the row of tubes, due to the "shadow effect" of the neighboring tubes.

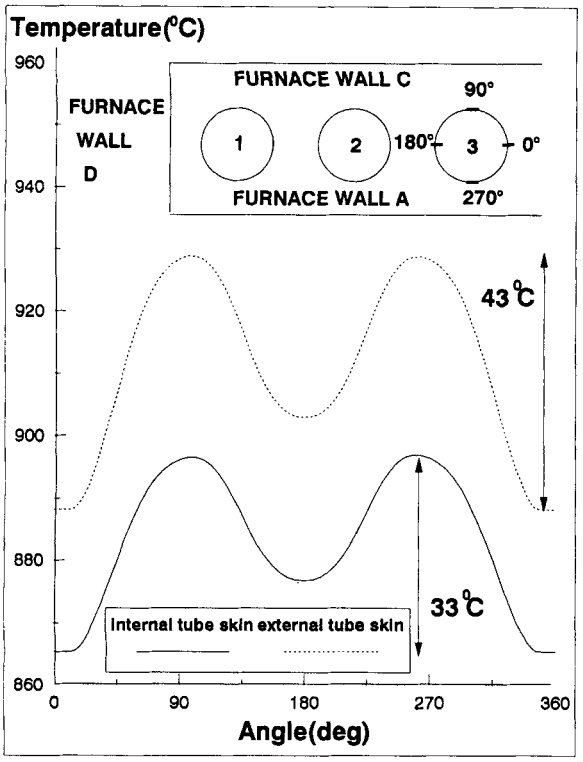

Figure 6. Circumferential tube skin temperature profiles.

Pass 3; height: 4 m from furnace floor.

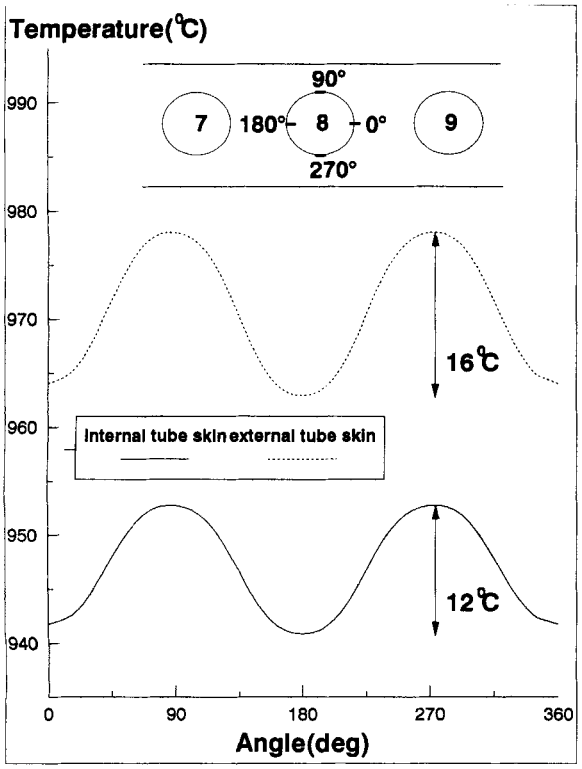

Figure 7. Circumferential tube skin temperature profiles.

Pass 8; height: 4 m from furnace floor.

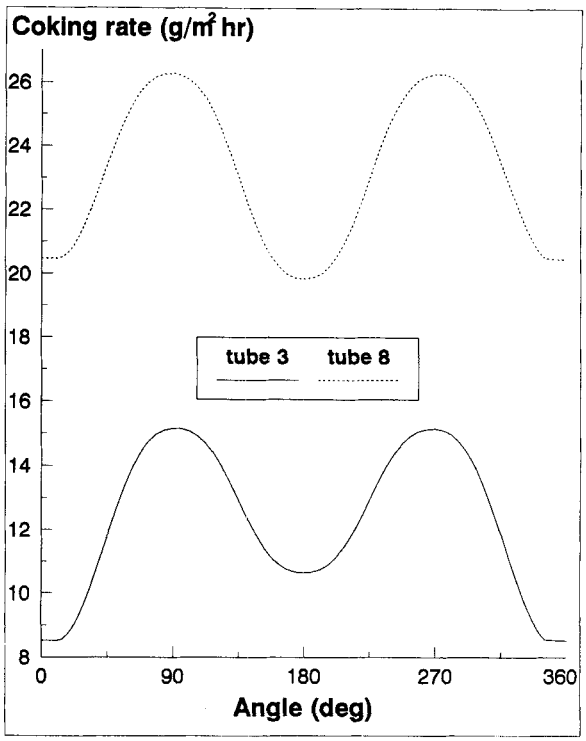

Figure 8. Circumferential coking rate profiles.

Pass 3 and pass 8; height: 4 m from furnace floor.

For the third tube, the local minimum calculated for the circumferential zones 4 and 5 (Figure 5) is 13°C higher than the absolute minimum calculated for the circumferential zones 1 and 8. This is explained by the proximity of the furnace wall D. The radiative heat transfer from the furnace side wall D to the circumferential zones 4 and 5 is much higher than that from the furnace side wall B to the circumferential zones 1 and 8. For the eighth tube, both minimum values are equal. The eighth tube is located in the center of the furnace, so that the distance between the circumferential zones 4 and 5 and the furnace wall D on the one hand and the circumferential zones 1 and 8 and the furnace wall B on the other hand is the same.

Through undesired side reactions, thermal cracking for olefins production is inevitably accompanied by coke formation. In early stages of the production cycle coke is formed by catalytic reactions whose rates depend upon the tube wall composition and morphology and, of course, temperature (Froment, 1990). Nonuniformities in the internal tube skin temperature therefore lead to nonuniform coking rates and coke layers. Figure 8 presents simulated circumferential initial coking rate profiles at the locations already dealt with in the Figures 6 and 7. The initial coking rates vary along the perimeter from 8 to 15 g/m^2 hr for the third pass and from 20 to 26 g/m^2 hr for the eighth pass.

These coking rates were calculated from kinetic equations coupled with the kinetic equations for the main reactions and are part of the CRACKSIM package.

The evolution with time of the coke layer thickness was illustrated by Plehiers et al. (1990), but requires substantial computing time. Anyway, the evolution with time would not substantially alter the shape of the circumferential profiles shown in Figure 8. From visual observations of cross sections of cracking tubes, it is well known that the coking layer thick-

Table 2. Characteristics of the Naphtha Cracking Furnace

Furnace	
Length	7,200 mm
Height	9,090 mm
Width	2,500 mm
Refractory thickness	230 mm
Insulation thickness	50 mm
Number of side wall burners	80
Firing conditions	
Heat input	21.49 MW
Reactor	
4 split coils	
Total coil length	53,885 mm
Number of passes	6
Internal diameter of passes 1-4	80 mm
Internal diameter of passes 5-6	114.3 mm
Wall thickness	7.8 mm
Operating conditions	
Feedstock	
Hydrocarbon feed rate per coil	2,785 kg/h
Steam dilution	0.7
Coil inlet temperature	620°C
Coil outlet pressure	1.8 atm
Material properties	
Viz Table 1	

ness is not uniform around the perimeter. Nonuniformities in the thickness of the coke layer evidently affects the run length of the production cycle. Furthermore, the decoking procedure, involving combustion of the coke by steam/air mixtures requires greater care, since excessive and detrimental temperatures may be generated in circumferential zones where the coke thickness is more important.

Circumferential tube skin nonuniformities can be reduced by using a larger tube pitch. The "shadow effect" is reduced, but the furnace dimensions increase. This problem is typical for radiative heat transfer, since heat source and heat sink have to "see" one another.

Simulation of a Naphtha Furnace with Staggered Rows of Coils

Furnace description

The main dimensions and operating conditions of the naphtha cracker with a staggered row configuration are given in Table 2. Figures 9 and 10 present a top and a front view of the furnace. It contains four split coils in a staggered row configuration, each making six passes through the furnace. The split part of the coils has four passes through the furnace.

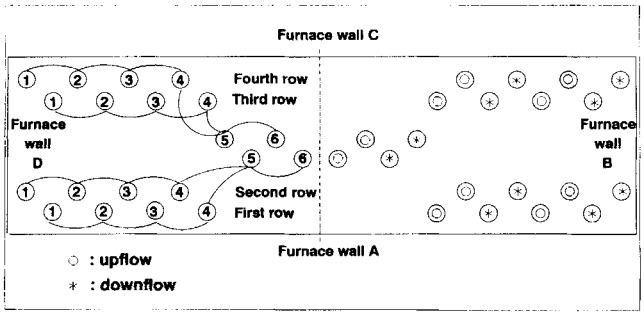

Figure 9. Top view of the naphtha furnace.

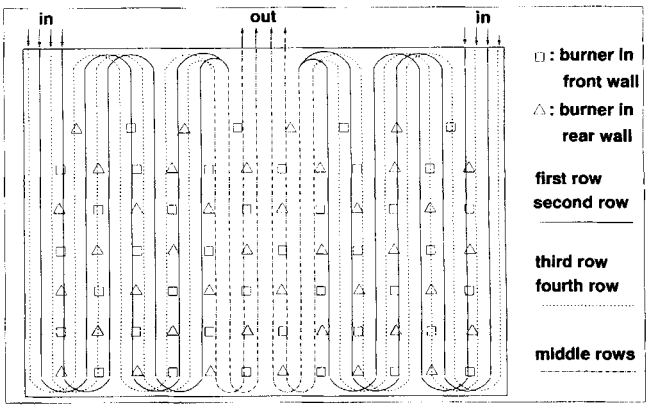

Figure 10. Front view of the naphtha furnace.

Because of symmetry, only two reactor coils had to be simulated.

The furnace is heated by 80 burners positioned in six rows of six burners and one row of four burners in both the front (A) and rear (C) wall. It was divided into zones by means of three equidistant horizontal planes. The four axial zones on the second pass of the first and the third row, and on the second and third pass of the second and the fourth row were circumferentially divided in eight equal zones (Figure 5). For lack of symmetry, all eight circumferential zones per axial division had to be simulated. Only three passes of each of the two simulated reactor coils were divided in circumferential direction in order to limit the total number of zones in the furnace and the required computer time. The number of external tube skin zones amount to 248, next to 14 furnace wall zones and four gas volume zones. A complete furnace simulation requires eight to ten hours CPU-time on a Data General AViiON 4120 (34 Mips).

Results and Discussion

Figures 11 and 12 show the calculated external and internal tube skin temperature profiles on the second pass of the first row and on the third pass of the fourth row at a height of 3.4 m from the furnace floor. Again important variations of the tube skin temperature along the tube perimeter are obtained. The external tube skin temperature for the second tube on the first row varies over 51°C from 872°C to 923°C.

Furthermore, the staggered row configuration leads to a second kind of "shadow effect," so that the two maximum values of the circumferential temperature profiles also differ. For the second pass of the first row, an absolute maximum temperature is obtained for the circumferential zones 6 and 7; these are the zones on the tube directly facing the furnace front wall (A). A local maximum is calculated for the circumferential zones 2 and 3. This maximum is lower because these zones are partly shielded from direct radiation from the rear wall (C) by the presence of the second, third and fourth row of tubes. The opposite is observed for the tube of the fourth row. The maximum temperature is now obtained for the zones 2 and 3 which directly face the rear wall (C). The circumferential zones 6 and 7 are now shielded from direct radiation from the front wall (A) by the first, second and third row of tubes.

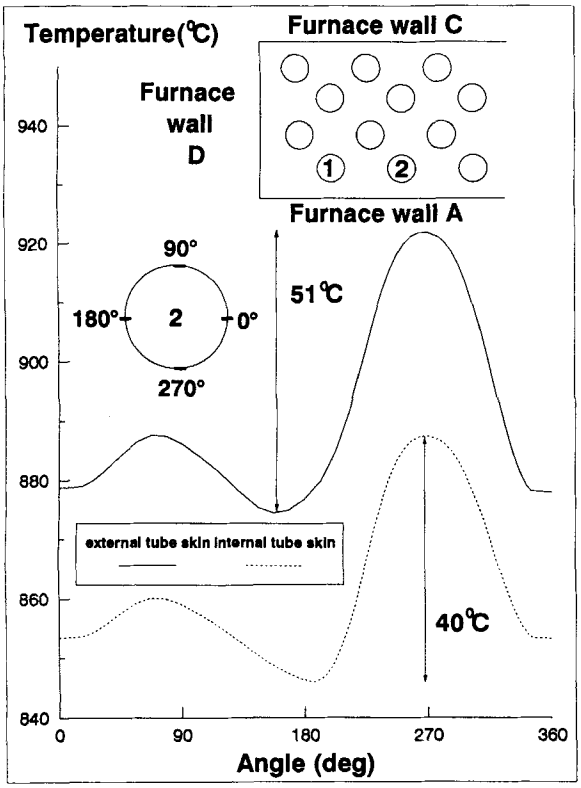

Figure 11. Circumferential tube skin temperature profiles.

Row 1; pass 2; height: 3.4 m from furnace floor.

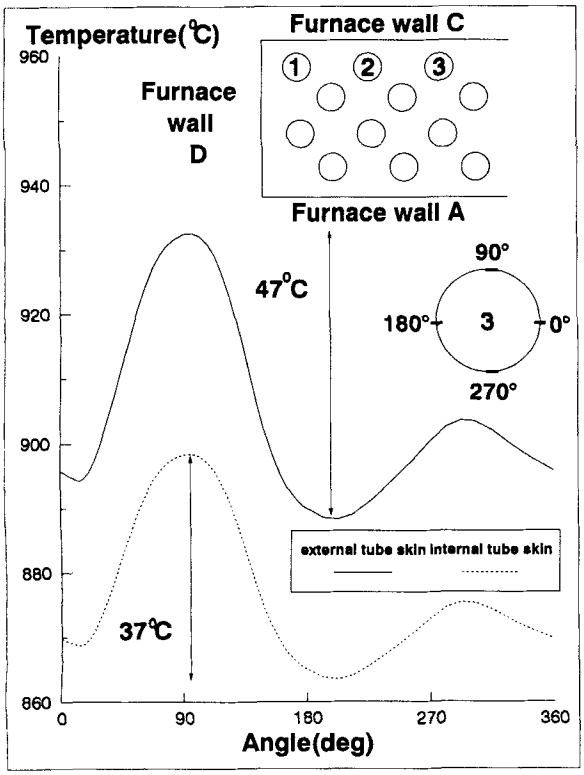

Figure 12. Circumferential tube skin temperature profiles.

Row 4; pass 3; height: 3.4 m from furnace floor.

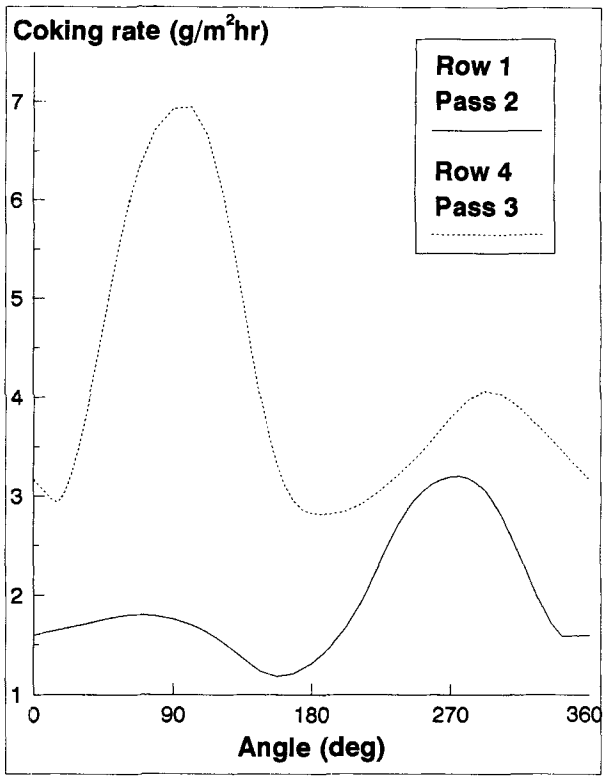

Figure 13. Circumferential coking rate profiles.

Row 1 pass 2; row 4 pass 3; height: 3.4 m from furnace floor.

Figure 13 presents the initial coking rate profiles corresponding to the tube skin temperature profiles shown in the Figures 11 and 12.

Conclusions

Nonuniformities of temperatures along the perimeter of the vertical coils of a cracking furnace were shown to be significant. Even with a single row of coils the difference between maxima and minima can be of the order of 50°C.

Yet, these differences cannot always be detected. Temperature measurements rely upon infrared pyrometry, through peepholes in the walls of the furnace, so that certain view angles only are possible.

Tube metal temperatures increase with time, as the heat-transfer resistance through the tube wall increases with growing thickness of the coke layer. The run length of the production cycle is often dictated by the maximum allowable tube metal temperature. The magnitude of the circumferential nonuniformities should be accounted for, so as to avoid excessive temperatures, detrimental to the tube metal life.

Uneven thickness of the coke layer also affects the pressure drop over the coil, another factor determining the run length of the production cycle. Excessive local restrictions may lead to a substantial pressure drop and reduced run lengths.

The nonuniformities also have to be accounted for in the decoking procedure, in order to avoid temperature excursions that might be detrimental to tube metal properties.

The model and computational scheme presented here can be used as a guide for plant operators and as a tool for those involved in the design of cracking furnaces.

Acknowledgment

Géraldine J. Heynderickx is grateful to the Belgian Nationaal Fonds voor Wetenschappelijk Onderzoek for a Research Assistantship.

Notation

A = surface of wall or tube zone (m^2)
c_{pj} = heat capacity of gas species (J/mol·K)
d_t = tube diameter (m)
E = black body emissive power (W/m^2)
F = molar flow rate (mol/s)
G = total mass flux of process gas ($kg/m^2 \cdot s$)
$-\Delta H$ = heat of reaction (J/mol)
h_p = process gas convection coefficient ($W/m^2 \cdot K$)
M_m = average molecular weight (g/mol)
n = stoichiometric coefficient
p_t = total pressure (Pa)
q = heat flux ($W/m^2 \cdot K$)
Q = heat flux (W/m^2)
r = tube radius (m)
r_r = reaction rate ($mol/m^3 \cdot s$)
R = gas constant (8.3143 J/mol·K)
R_b = radius of tube bend (m)
Re = Reynolds number
T = temperature (K)
z = axial reactor coordinate (m)
Z_iZ_j = total exchange area between zones i and j (m^2)

Greek letters

α = unit conversion factor
θ = tube perimeter angle (rad) (Figure 5)
Λ = tube bend angle (°)
λ = tube material conductivity (W/m·K)
σ = Stefan-Boltzmann constant ($5.7\ 10^{-8}\ W/m^2 \cdot K^4$)

Literature Cited

Clymans, P. J., and G. F. Froment, "Computer Generation of Reaction Paths and Rate Equations in the Thermal Cracking of Normal and Branched Paraffins," *Comput. and Chem. Eng.*, **8**(2), 137 (1984).

Froment, G. F., "Coke Formation in the Thermal Cracking of Hydrocarbons," *Rev. in Chem. Eng.*, **6**(4), 295 (1990).

Froment, G. F., and K. B. Bischoff, *Chemical Reactors Analysis and Design*, John Wiley and Sons, New York (1990).

Hillewaert, L. P., J. L. Dierickx, and G. F. Froment, "Computer Generation of Reaction Schemes and Rate Equations for Thermal Cracking," *AIChE J.*, **34**(1), 17 (1988).

Hottel, H. C., "Radiant Heat Transmission," *Trans. Am. Soc. Mech. Engrs.*, **53**, 265 (1931).

Hottel, H. C., and A. F. Sarofim, *Radiative Heat Transfer*, McGraw-Hill, New York (1967).

Plehiers, P. M., and G. F. Froment, "Firebox Simulation of Olefin Units," AIChE National Spring Meeting, New Orleans, LA (1988).

Plehiers, P. M., and G. F. Froment, "Firebox Simulation of Olefin Units," *Chem. Eng. Commun.*, **80**, 81 (1989).

Plehiers, P. M., G. C. Reyniers, and G. F. Froment, "Simulation of the Run Length of an Ethane Cracking Furnace," *Ind. Eng. Chem. Res.*, **19**, 636 (1990).

Rao, M. V. R., P. M. Plehiers, and G. F. Froment, "The Coupled Simulation of Heat Transfer and Reaction in a Pyrolysis Furnace," *Chem. Eng. Sci.*, **43**, 1223 (1988).

Vercammen, H. A. J., and G. F. Froment, "Simulation of Thermal Cracking Furnaces," *ACS Symp. Ser.*, No. 65, *Chemical Reaction Engineering*, V. W. Weekman and D. Luss, eds., pp. 271-281 (1978).

Vercammen, H. A. J., and G. F. Froment, "An Improved Zone Method for the Simulation of Radiation in Industrial Furnaces," *Int. J. Heat Transf.*, **23**, 329 (1980).

Willems, P., and G. F. Froment, "Kinetic Modeling of the Thermal Cracking of Hydrocarbons, Part 1: Calculation of Frequency Factors," *Ind. Eng. Chem. Res.*, **27**, 1959 (1988).

Willems, P., and G. F. Froment, "Kinetic Modeling of the Thermal Cracking of Hydrocarbons, Part 2: Calculation of Activation Energies," *Ind. Eng. Chem. Res.*, **27**, 1966 (1988).

Manuscript received Mar. 11, 1992, and revision received June 26, 1992.